Time-varying multiplex network: Intralayer and interlayer synchronization

Sarbendu Rakshit,[1] Soumen Majhi,[1] Bidesh K. Bera,[1] Sudeshna Sinha,[2] and Dibakar Ghosh[1,*]
[1]*Physics and Applied Mathematics Unit, Indian Statistical Institute, 203 B. T. Road, Kolkata-700108, India*
[2]*Indian Institute of Science Education and Research Mohali, Manauli P.O. 140 306, Punjab, India*
(Received 6 July 2017; published 15 December 2017)

A large class of engineered and natural systems, ranging from transportation networks to neuronal networks, are best represented by multiplex network architectures, namely a network composed of two or more different layers where the mutual interaction in each layer may differ from other layers. Here we consider a multiplex network where the intralayer coupling interactions are switched stochastically with a characteristic frequency. We explore the intralayer and interlayer synchronization of such a time-varying multiplex network. We find that the analytically derived necessary condition for intralayer and interlayer synchronization, obtained by the master stability function approach, is in excellent agreement with our numerical results. Interestingly, we clearly find that the higher frequency of switching links in the layers enhances both intralayer and interlayer synchrony, yielding larger windows of synchronization. Further, we quantify the resilience of synchronous states against random perturbations, using a global stability measure based on the concept of basin stability, and this reveals that intralayer coupling strength is most crucial for determining both intralayer and interlayer synchrony. Lastly, we investigate the robustness of interlayer synchronization against a progressive demultiplexing of the multiplex structure, and we find that for rapid switching of intralayer links, the interlayer synchronization persists even when a large number of interlayer nodes are disconnected.

DOI: 10.1103/PhysRevE.96.062308

I. INTRODUCTION

The theory of complex networks provides a comprehensive way to describe the universal properties and collective features emerging from the interaction of a large number of dynamical units, in systems ranging from the human brain to human society. In such large interactive systems, the collective dynamics is rich and nontrivial, depending significantly on the type of interaction and the network structure of the connections. Now, in recent decades, a lot of attention has been devoted to studying *static* networks where the underlying connections do not evolve over time. However, in many real networks, the interactional arrangement is not static. Rather, they are dynamically structured, with connections appearing, disappearing, or switching at different time scales [1]. For instance, in social interaction networks [2], the social relationship or communication between pairs of individuals changes continuously, and so links are continuously created or terminated or changed. So a temporal progression of links is an inherent feature of several natural and artificial networks [3], and a static approximation to such systems is valid only when the changes in links occur over extremely long time scales. In this context, recent research has focused on the emergence of *synchronization* in a time-varying complex network [4–10]. This is very crucial because of its enormous applicability in several fields, including consensus problems [11], disease spreading [12], power transmission systems [13], functional brain networks [14], person-to-person communication [15], and even in the process of chemotaxis [16] and wireless sensor networks [17].

In another development, it emerged that *multilayered* networks, such as multiplex networks, provide a very important network architecture for the realistic description of a large class of systems, where processes occurring in a network may affect other networks as well [18,19]. Such networks are composed of two or more distinct layers, where the mutual interaction in each layer may differ from other layers. For instance, social networks where different communities are tied and affiliated by different types of relations [20], mobility networks where the individual entities may be served by different types of transports [21], air transportation networks [22], subway networks [23], and neuronal networks [24] are best represented by the multilayered framework. So the multilayered network structure has assisted in the understanding of several collective properties that emerge due to the interconnections in complex systems [25,26], such as epidemic spreading processes [27–30], diffusion [31], controllability [32], percolation [33,34], evolutionary game dynamics [35], and congestion in traffic [36]. Importantly, results on multiplex networks have been found to be significantly different from the monolayer case. Specifically, different types of synchronization have been studied in the multilayered network formulation, such as explosive synchronization [37], intra- and interlayer synchronization [38–40], cluster synchronization [41], chimera states [42–44], and breathing synchronization [45]. Apart from these types of synchronization, several global synchronous states have been identified by using coupling through different state variables [46], interplaying layer topologies coordination [47], and such states have also been detected in interconnected layers in smart grids [48] and in a networks configuration [49].

However, in all previous studies the synchronous states have been investigated either in completely time-static networks having multilayer construction, or in time-evolving networks on the top of a single layer. Motivated by this, here we study the synchronization in a multiplex network consisting of two layers possessing time-varying links. Generally, a multiplex network structure is characterized by nodes having two different types of links. The first type establishes an intracoupling

*dibakar@isical.ac.in

interaction between the nodes located in the same layer. The second type refers to the intercoupling interaction of the dynamic elements between the layers. In this work, we consider that the former interaction changes in time while the second type of interaction is time-invariant. Such a scenario describes, for instance, a biological network in which two classes of species interact through a common medium. Each class evolves in time, and consequently their interactions are time-varying, while the connection between the classes is preserved. A time-varying multilayered structure also offers a good model to represent communication networks, social networks [50], the world wide web, and the epidemic spreading process [51].

In our work, we will focus on two types of synchronization in multiplex networks composed of time-varying layers: intralayer and interlayer synchronization. Intralayer synchronization is defined as the state of synchrony in each of the individual layers, irrespective of the synchrony between the replica nodes. On the other hand, interlayer synchronization corresponds to the case of synchrony between all the replica nodes regardless of intralayer synchronization in the multiplex network. We derive analytically the necessary condition for intralayer and interlayer synchronization using linear stability analysis. However, linear stability analysis reflects only local stability, and it is valid only for infinitesimally small perturbations around the synchronization manifold, thus failing to characterize the stability against significantly large perturbations. So for quantification of global stability, we adopt the *basin stability* [52] paradigm, which is a nonlocal and nonlinear measure and is related to the volume of the basin of attractions. The basin stability measure has been used successfully to analyze the stability of high-dimensional systems and for the quantification of different stable steady states in coupled delayed [53] and nondelayed systems [54], synchronized states [5], and chimera states [55]. Further, we extend our work on the quantification of the robustness of interlayer synchronization by studying the changes in basin stability against the random removal of the interlayer connections over time.

Our paper is organized as follows: Section II is devoted to a brief description of the proposed multiplex network. Intralayer and interlayer synchronization under varying coupling strengths, for different rewiring frequencies, is discussed in Sec. III. In Sec. III A, we present the analytical condition for synchronization obtained through linear stability analysis. In Sec. III B, we show the effect of varying coupling strengths and rewiring frequencies on the global basin stability measure. Next we investigate the effect of demultiplexing on the synchronized state. Lastly, Sec. IV provides a discussion of our analytical and numerical results.

II. DYNAMICS OF THE TIME-VARYING MULTIPLEX NETWORK

We consider the two layers where each layer is composed of N nodes of m dimensional identical dynamical systems. The states of the layers are represented by the vectors $\mathbf{X} = \{\mathbf{x}_1, \mathbf{x}_2, \ldots, \mathbf{x}_N\}$ and $\mathbf{Y} = \{\mathbf{y}_1, \mathbf{y}_2, \ldots, \mathbf{y}_N\}$ with $\mathbf{x}_i, \mathbf{y}_i \in \mathbb{R}^m$ for $i = 1, 2, \ldots, N$. In our prescribed model, the intralayer coupling topologies are time-varying small-world networks encoded by the Laplacian matrices $\mathscr{L}^1$ and $\mathscr{L}^2$, respectively. The small-world network is constructed by following the procedure proposed by Watts and Strogatz in [56]. We commence with N nodes with regular ring coupling topology, where each node is connected to its $2k$ nearest neighbors, k on each side. Then with probability p, we reconnect all the initial edges to vertices chosen uniformly at random from distant nodes, with dual edges impermissible. Now the links in both layers vary over time through the rewiring of each link in the entire network stochastically and independently, with an average frequency f, while the interlayer connections are preserved over time. Particularly, at any time t, given time step dt, we rewire each layer by constructing a new small-world network from the initial ring, independently, with probability $f\,dt$. Now the successively created small-world networks will be statistically equivalent due to the choice of fixed parameters k and p throughout the procedure. Large f indicates very fast switching of links, implying that the networks change rapidly, whereas small f implies that the two layers are almost static, as the links have a very low probability of change.

The dynamics of the ith nodes of both layers are described by the given set of equations:

$$\begin{aligned} \dot{\mathbf{x}}_i &= F(\mathbf{x}_i) - \epsilon \sum_{j=1}^{N} \mathscr{L}_{ij}^1 G(\mathbf{x}_j) + \lambda[H(\mathbf{y}_i) - H(\mathbf{x}_i)], \\ \dot{\mathbf{y}}_i &= F(\mathbf{y}_i) - \epsilon \sum_{j=1}^{N} \mathscr{L}_{ij}^2 G(\mathbf{y}_j) + \lambda[H(\mathbf{x}_i) - H(\mathbf{y}_i)], \end{aligned} \tag{1}$$

where $F : \mathbb{R}^m \to \mathbb{R}^m$, $G : \mathbb{R}^m \to \mathbb{R}^m$, and $H : \mathbb{R}^m \to \mathbb{R}^m$ represent the vector field of the system evolution and the output vectorial function within the layers and between the layers, respectively. Parameters ϵ and λ are the intralayer and interlayer coupling strengths, respectively. Here $\mathscr{L}_{ij}^{1,2}$ are the zero-row sum Laplacian matrices. These Laplacian matrices are obtained from the adjacent matrices $\mathscr{A}^{1,2} = (\mathscr{A}_{ij}^{1,2})_{N\times N}$ with $\mathscr{A}_{ij}^{1,2} = 1$ if the ith node and the jth node are connected and zero otherwise; the diagonal elements $\mathscr{L}_{ii}^{1,2}$ are the sum of the corresponding rows of $\mathscr{A}^{1,2}$, and the off-diagonal elements are the negative of the corresponding elements in the adjacent matrices, i.e., $\mathscr{L}_{i,j}^{1,2} = -\mathscr{A}_{i,j}^{1,2} (i \neq j)$ and $\mathscr{L}_{i,i}^{1,2} = \sum_{j=1}^{N} \mathscr{A}_{i,j}^{1,2}$.

For revealing the mechanisms underlying the emergence of different collective phenomena in complex systems, coupled oscillatory systems offer a generic test-bed for investigation. So in the sections below, we will explore the behavior of time-varying multiplex networks, where the nodal dynamics is given by nonlinear Rössler oscillators. Our main emphasis will be to identify the parameter regions for intralayer and interlayer synchronization, under variation of the following parameters: (i) intralayer and interlayer coupling strengths, (ii) rewiring frequency f, and (iii) total number of nearest-neighbor links $2k$.

III. RESULTS

We consider the above multiplex network (1), where the layers are composed by Rössler oscillators, with its

autonomous evolution $F(\mathbf{x})$ in the following form:

$$\mathbf{F}(\mathbf{x}) = \begin{pmatrix} -y - z \\ x + ay \\ b + z(x - c) \end{pmatrix}, \tag{2}$$

where $a = 0.1$, $b = 0.1$, and $c = 14.0$. For this set of parameter values, an isolated Rössler oscillator retains chaotic behavior. We take the intralayer and interlayer coupling functions as diffusive through the variable y, i.e., $G(\mathbf{x}) = (0, y, 0)'$ and $H(\mathbf{x}) = (0, y, 0)'$, where $(\cdot)'$ denotes the transpose of the matrix.

We start by examining the synchronization error under variation of the intralayer and interlayer coupling strengths. We consider the intralayer coupling strength ϵ to be much larger than the interlayer coupling strength λ, and specifically we will consider $\epsilon = 6\lambda$, with no loss of generalization. The simulations presented here are obtained for $N = 200$ oscillators in each layer, the number of nearest neighbors on each side, $k = 3$, and the fraction of random links, $p = 0.1$. We integrate our network (1) numerically using the fifth-order Runge-Kutta-Fehlberg integration algorithm scheme with a time step of 0.01.

The intralayer and interlayer synchronization errors are, respectively, defined as

$$E_{\text{intra}} = \lim_{T\to\infty} \frac{1}{T} \int_0^T \sum_{j=2}^{N} \frac{\|\mathbf{x}_j(t) - \mathbf{x}_1(t)\|}{N-1} dt \tag{3}$$

and

$$E_{\text{inter}} = \lim_{T\to\infty} \frac{1}{T} \int_0^T \sum_{j=1}^{N} \frac{\|\delta\mathbf{z}_i(t)\|}{N} dt, \tag{4}$$

where $\delta\mathbf{z}_i(t) = \mathbf{y}_i(t) - \mathbf{x}_i(t)$ is the difference between the layer dynamics, $\|\cdot\|$ denotes the Euclidean norm, and T is the long-time interval. To calculate the intralayer and interlayer synchronization errors, the time interval is taken over 1×10^5 units after an initial transient of 2×10^5 units. The final state is considered synchronized if the corresponding synchronization error is less than 10^{-6}, otherwise the system is in a desynchronized state.

In Fig. 1(a), the intralayer synchronization error E_{intra} is plotted with respect to the intralayer coupling parameter ϵ for several values of the rewiring frequency f of the network layers. For smaller values of the rewiring frequency, $f = 0.001$ (i.e., when the two layers are almost static), the intralayer synchronization is sustained over the range $0.51 \leqslant \epsilon \leqslant 2.0$. Increasing the value of f to 0.01 increases the range of ϵ for which intralayer synchronization occurs to $0.46 \leqslant \epsilon \leqslant 2.14$. For very rapidly changing layers, such as when the probability of switching links $f = 10$, the intralayer synchronization occurs in an even larger range of coupling strengths: $0.26 \leqslant \epsilon \leqslant 3.1$. So it is evident from this figure that a *higher frequency of switching links in the layers enhances intralayer synchrony*, and it enlarges the range of coupling strengths yielding intralayer synchronization as compared to static networks.

In a similar fashion, we obtain the interlayer synchronization error E_{inter} under varying coupling strengths for different values of rewiring frequencies f [cf. Fig. 1(b)].

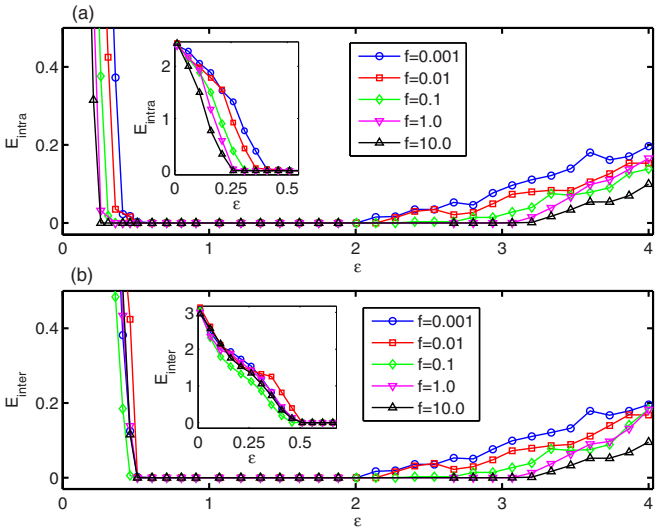

FIG. 1. Variation of (a) intralayer and (b) interlayer synchronization errors with respect to the intralayer coupling parameter ϵ (interlayer coupling strength $\lambda = \frac{\epsilon}{6}$) for different values of rewiring frequencies $f = 0.001$ (blue circle), 0.01 (red square), 0.1 (green diamond), 1.0 (magenta lower triangle), and 10 (black upper triangle). The insets in the respective panels show the magnified version of errors for a better visualization.

The interlayer synchronization error E_{inter} first decreases for increasing values of coupling strength, and it becomes zero, indicating complete synchronization, as ϵ crosses a certain threshold. This value of critical coupling is not very sensitive to the frequency of switching links in the layers.

Furthermore, notice that as the coupling strength increases beyond a critical value, the network loses synchrony again. The critical coupling strength at which this desynchronization occurs depends on f. Higher values of f provide longer persistence of synchrony, that is, rapidly changing links in the layers yield larger windows of synchronization. It is important to note that for $\epsilon \geqslant 0.5$, intralayer and interlayer synchronization occurs for all values of f, and the entire network is synchronized in a global sense.

A. Linear stability analysis

Now we analytically derive the necessary conditions for intralayer and interlayer synchronization in the multiplex network given by Eq. (1) using the master stability function (MSF) approach. For intralayer synchronization, we only consider the synchrony of the oscillators in the two layers, irrespective of synchrony between the replica nodes. For this, if $\mathbf{x}(t)$ and $\mathbf{y}(t)$ are the synchronization manifolds of the two layers, then $\mathbf{x}_i(t) = \mathbf{x}(t)$ and $\mathbf{y}_i(t) = \mathbf{y}(t)$, $i = 1, 2, \ldots, N$. Let $\delta\mathbf{x}_i(t)$ and $\delta\mathbf{y}_i(t)$ be the deviation from synchronization manifolds, i.e., $\mathbf{x}_i(t) = \mathbf{x}(t) + \delta\mathbf{x}_i(t)$ and $\mathbf{y}_i(t) = \mathbf{y}(t) + \delta\mathbf{y}_i(t)$. Then the perturbed linearized equations become

$$\begin{aligned} \delta\dot{\mathbf{x}}_i = {} & JF(\mathbf{x})\delta\mathbf{x}_i - \epsilon \sum_{j=1}^{N} \mathscr{L}^1_{ij} JG(\mathbf{x})\delta\mathbf{x}_j \\ & + \lambda[JH(\mathbf{y})\delta\mathbf{y}_i - JH(\mathbf{x})\delta\mathbf{x}_i] \end{aligned} \tag{5}$$

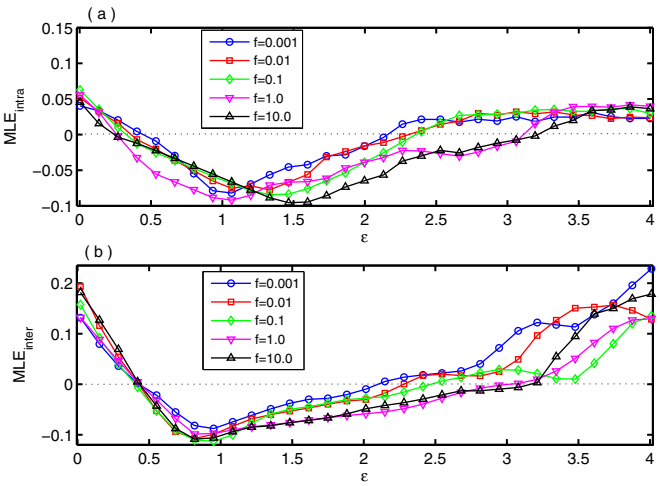

FIG. 2. Maximum Lyapunov exponent corresponding to (a) intralayer synchronization and (b) interlayer synchronization with respect to the parameter ϵ where $\lambda = \frac{\epsilon}{6}$ for the same set of rewiring frequencies as in Fig. 1.

and

$$\delta\dot{\mathbf{y}}_i = JF(\mathbf{y})\delta\mathbf{y}_i - \epsilon\sum_{j=1}^{N}\mathscr{L}_{ij}^2 JG(\mathbf{y})\delta\mathbf{y}_j + \lambda[JH(\mathbf{x})\delta\mathbf{x}_i - JH(\mathbf{y})\delta\mathbf{y}_i], \tag{6}$$

where J denotes the Jacobian operator and $(\mathbf{x},\mathbf{y}) = (\tilde{\mathbf{x}},\tilde{\mathbf{y}})$ is the state of the coupled system,

$$\begin{aligned}\dot{\tilde{x}} &= F(\tilde{\mathbf{x}}) + \lambda[H(\tilde{\mathbf{y}}) - H(\tilde{\mathbf{x}})],\\ \dot{\tilde{y}} &= F(\tilde{\mathbf{y}}) + \lambda[H(\tilde{\mathbf{x}}) - H(\tilde{\mathbf{y}})].\end{aligned} \tag{7}$$

Now we calculate all the Lyapunov exponents transverse to the synchronization manifolds $\mathbf{x}_i(t) = \mathbf{x}(t)$ and $\mathbf{y}_i(t) = \mathbf{y}(t)$ by solving the coupled linearized systems (5) and (6) together with nonlinear coupled systems (7). Let $\lambda_{\max}^{(1)}$ and $\lambda_{\max}^{(2)}$ be the maximum Lyapunov exponents (MLEs) of the two layers. Intralayer synchronization occurs if the maximum of these two Lyapunov exponents, i.e., $\mathrm{MLE_{intra}} = \max\{\lambda_{\max}^{(1)},\lambda_{\max}^{(2)}\}$, is negative. The variation of $\mathrm{MLE_{intra}}$ by changing the coupling strength ϵ gives the necessary condition for the stability of the intralayer synchronization state when $\mathrm{MLE_{intra}} < 0$.

To confirm the validity of the analytical stability condition obtained above for intralayer synchronization, we plot $\mathrm{MLE_{intra}}$ with respect to ϵ for several values of rewiring frequencies f. The dependence of the rewiring frequency f is included in the linearized systems (5) and (6) through the Laplacian matrices $\mathscr{L}^1$ and $\mathscr{L}^2$. The number of changes of the Laplacian matrices depends on the value of f. For higher values of f, the Laplacian matrices change rapidly, whereas for lower f they remain almost invariant. Figure 2(a) depicts the variation of $\mathrm{MLE_{intra}}$ by changing ϵ for the same set of rewiring frequencies, and that turns out to be negative exactly at the values of ϵ where $\mathrm{E_{intra}}$ vanishes in Fig. 1(a). For a further increase in ϵ, $\mathrm{MLE_{intra}}$ becomes positive due to short-wavelength bifurcation [57], and this is exactly where $\mathrm{E_{intra}}$ becomes nonzero again in Fig. 1(a). With higher f, $\mathrm{MLE_{intra}}$ declines to zero faster and remains negative for much larger intervals of ϵ.

For the stability condition of the interlayer synchronization state, let $\delta\mathbf{z}_i = \mathbf{y}_i - \mathbf{x}_i$ be the small perturbation of the ith replica from its synchronization manifold $\mathbf{x}_i = \mathbf{y}_i$. Then the linearized equation near the interlayer synchronization manifold becomes

$$\delta\dot{\mathbf{z}}_i = [JF(\tilde{\mathbf{x}}_i) - 2\lambda JH(\tilde{\mathbf{x}}_i)]\delta\mathbf{z}_i - \epsilon\sum_{j=1}^{N}\mathscr{L}_{ij}^2 JG(\tilde{\mathbf{x}}_j)\delta\mathbf{z}_j + \epsilon\sum_{j=1}^{N}\Delta L_{ij}G(\tilde{\mathbf{x}}_j), \tag{8}$$

where $\Delta L_{ij} = \mathscr{L}_{ij}^1 - \mathscr{L}_{ij}^2$ is the difference between the two Laplacian matrices and $\tilde{\mathbf{x}}_i$ is the state of the ith node in an isolated layer evolving according to

$$\dot{\tilde{x}}_i = f(\tilde{\mathbf{x}}_i) - \epsilon\sum_{k=1}^{N}\mathscr{L}_{ik}^1 G(\tilde{\mathbf{x}}_k). \tag{9}$$

The influence of the last term on the right-hand side of Eq. (8) in driving the system away from the interlayer synchronization manifold is maximum when the topology of the two layers is significantly different. But it can be expected that when the difference between the two topologies is very small, the MSF approach for stability of interlayer synchronization is applicable [40]. In our case, the rewiring frequency f, the link rewiring probability p, and the average degree of the two layers are identical, so the difference between two Laplacian matrices ΔL_{ij} is almost negligible. So according to the MSF approach, the negativity of the maximum Lyapunov exponent $\mathrm{MLE_{inter}}$ obtained from linearized Eq. (8) together with nonlinear Eq. (9) implies stable interlayer synchronization.

Figure 2(b) shows the variation of $\mathrm{MLE_{inter}}$ under changing coupling strength ϵ for several values of f. The $\mathrm{MLE_{inter}}$ curves of interlayer synchronization decrease to zero and become negative approximately at $\epsilon = 0.51$, irrespective of the value of f. However, the MLE's cross zero again at values of ϵ that are strongly dependent on f. These trends completely corroborate the numerical results displayed in Fig. 1(b).

B. Basin stability measure

The linear stability analysis presented above is valid only for small perturbations from the synchronization manifold. However, the perturbation may not be infinitesimal, and in that case the stability condition for the existence of synchronization using linear stability analysis is necessary, but not sufficient. To quantify how stable a synchronization state is against large perturbations, we use the concept of basin stability (BS), which is a nonlinear and nonlocal approach that concentrates on the volume of the basin of attraction rather than the traditional linearization-based approach. It is easily applicable even to higher-dimensional complex systems and a robust gadget for characterizing multistable states. For numerical computation of BS, we integrate the multiplex network (1) for Q different states distributed randomly over a prescribed phase-space volume (with Q being sufficiently large), and we follow the evolution of the system from different initial states quite far from synchronization. If M number of states finally arrive at

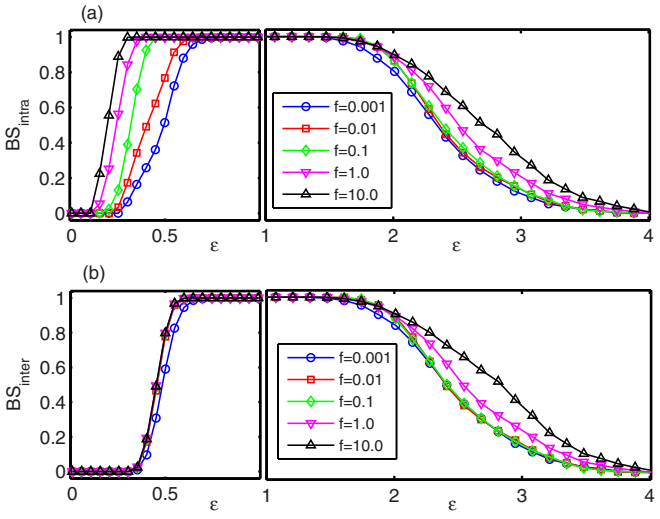

FIG. 3. Variation of basin stability for (a) intralayer and (b) interlayer synchronous state with respect to the parameter ϵ where $\lambda = \frac{\epsilon}{6}$ with different values of rewiring frequencies: $f = 0.001$ (blue circle), $f = 0.01$ (red square), $f = 0.1$ (green diamond), $f = 1.0$ (magenta lower triangle), and $f = 10$ (black upper triangle).

the synchronous state, then the BS for the synchronous state is estimated as $\frac{M}{Q}$. The value of BS lies in the range $[0,1]$, with $\mathrm{BS} = 0$ implying that for all random initial conditions the synchronized state is unstable, while it is globally stable for any nonlocal perturbation when $\mathrm{BS} = 1$. When $0 < \mathrm{BS} < 1$, the value of BS reflects the probability of recovering the synchronous state from perturbations for a typical random initial condition in the prescribed phase-space volume. For instance, using BS analysis, we will show that there exist finite windows of coupling strengths in which the fraction of perturbed states that revert to complete intralayer and interlayer synchronization is nonzero, but less than 1. So this measure complements the information obtained through linear stability analysis.

Specifically in this work, to calculate BS we have integrated the entire system for $Q = 1000$ different initial conditions from the prescribed phase-space volume $[-20,20] \times [-20,20] \times [0,35]$. Figure 3 shows the change in BS for the intralayer and interlayer synchronous states, under variation of the coupling parameter ϵ, for different values of rewiring frequencies f. The BS of the intralayer and interlayer synchronized states is denoted as $\mathrm{BS}_{\mathrm{intra}}$ and $\mathrm{BS}_{\mathrm{inter}}$, respectively.

Figure 3(a) shows the variation of $\mathrm{BS}_{\mathrm{intra}}$ with respect to the coupling strength ϵ for several representative values of rewiring frequency f. At low rewiring frequencies, for instance $f = 0.001$, the $\mathrm{BS}_{\mathrm{intra}}$ estimate shows that intralayer synchronization is not possible in the range $0 < \epsilon < 0.25$ for any initial condition lying in the prescribed phase-space volume. When coupling strength ϵ increases to the range $[0.25 \leqslant \epsilon \leqslant 0.7]$, the value of $\mathrm{BS}_{\mathrm{intra}}$ increases to values greater than zero (but less than 1), implying that the probability of getting intralayer synchronization increases for randomly chosen initial conditions. From linear stability analysis, one concluded that intralayer synchronization is only possible for $0.51 \leqslant \epsilon \leqslant 2.0$ as in Fig. 2(a). However, using basin stability analysis, it can be observed that intralayer synchronization does occur for some fraction of randomly chosen initial conditions in the prescribed phase-space volume, for coupling strengths $\epsilon \geqslant 0.25$. For $0.7 < \epsilon < 1.74$, the value of $\mathrm{BS}_{\mathrm{intra}}$ is unity, which signifies that the intralayer synchronized state is a global attractor of the dynamics. Further increase in the value of ϵ to the interval $[1.74,3.35]$ leads $\mathrm{BS}_{\mathrm{intra}}$ to again decrease below 1, signifying that only a fraction (greater than 0 and less than 1) of initial conditions yield intralayer synchronization. Similar trends are seen for higher rewiring frequencies f, such as $f = 0.1,1.0,10.0$, as displayed in Fig. 3(a). Here again, $\mathrm{BS}_{\mathrm{intra}}$ starts with the minimum value of zero and increases sharply with increasing ϵ, reaching the maximum value unity. Note that for a slower rewiring of links, such as $f = 0.001$ and 0.01, $\mathrm{BS}_{\mathrm{intra}}$ increases more gradually and approaches unity at higher values of coupling strength ϵ. Higher coupling strength ϵ leads the full basin to support synchrony in the layers, and this scenario is realized irrespective of the value of f. However, in the transition from synchrony to incoherence, BS decreases in a gradual manner, no matter how rapidly the links in the layers change. *The remarkably different values of* $\mathrm{BS}_{\mathrm{intra}}$ *for different rewiring frequencies* f *underscores the impact of the rewiring frequency on intralayer synchronization.*

Figure 3(b) shows $\mathrm{BS}_{\mathrm{inter}}$ as a function of ϵ. Here, $\mathrm{BS}_{\mathrm{inter}}$ increases rapidly at the same value of ϵ for almost all f. This is in concurrence with the trends already observed from synchronization errors [cf. Fig. 1(b)]. Here the increase of $\mathrm{BS}_{\mathrm{inter}}$ from 0 to 1 is not significantly different for different f. $\mathrm{BS}_{\mathrm{inter}}$ remains unity in a window of global synchronization. However, further increasing ϵ results in a gradual decrease in $\mathrm{BS}_{\mathrm{inter}}$ to zero at $\epsilon \sim 4.0$. The decrease in basin stability depends on the rewiring frequency f, as it did for the case of $\mathrm{BS}_{\mathrm{intra}}$. Notably, basin stability of the intralayer and interlayer synchronization is neither 0 nor 1 at the threshold value of ϵ for which synchrony appeared for small perturbations around the synchronous state [cf. Figs. 1(a) and 1(b)]. Rather, some fraction of states evolves to the synchronized state at the critical value of ϵ.

To explore the complete scenario of intralayer and interlayer synchronization, for a specific rewiring frequency f, we compute the intralayer and interlayer synchronization errors for the network for different intralayer and interlayer coupling strengths in the ϵ-λ plane. Specifically, we consider intralayer coupling strength $\epsilon \in [0,4]$ and interlayer coupling strength $\lambda \in [0,2]$, and Figs. 4(a) and 4(b) show the intralayer and interlayer synchronization errors in the ϵ-λ plane. From Fig. 4(a) it is evident that below a critical value of ϵ ($\epsilon < 0.35$), intralayer synchronization does not occur for any value of λ. Beyond that, we observe intralayer synchronization over a certain range of intralayer coupling strengths ϵ, and this range is almost independent of the interlayer coupling strength λ. Similar trends are observed for the case of interlayer synchronization error E_{inter}, shown in Fig. 4(b), except it requires both ϵ and λ to exceed certain values to induce interlayer synchronization. Figures 4(c) and 4(d) show the basin stability measure in the ϵ-λ plane. It is clear from these that the transition from desynchronization to intralayer and interlayer synchronization is almost "vertical" in the figures, implying that the transition occurs at critical values of intralayer coupling strength ϵ that are nearly independent of the

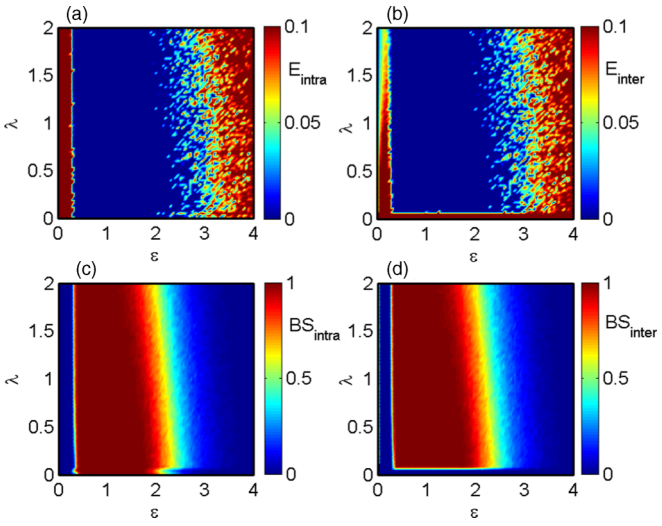

FIG. 4. Synchronization errors (first row) and basin stability measures (second row) in the ϵ-λ plane for (a), (c) intralayer synchronization and (b), (d) interlayer synchronization. Here $f = 0.1$.

interlayer coupling strength λ. So this suggests that intralayer coupling strength plays the most crucial role in determining the stability of both intralayer and interlayer synchronous states.

Further, we explore the effect of k (i.e., the number of nearest neighbors on either side) on intralayer and interlayer synchronization. Figures 5(a) and 5(b) show the fraction of random initial conditions leading to intralayer and interlayer synchronization, under variation of rewiring frequency f and intralayer coupling strength ϵ, for $k = 2$ (i.e., four neighbors). Clearly, the region of coupling strength ϵ supporting synchronization increases as the rewiring frequency f increases. However, as the number of neighbors increases, such as for $k = 3$ (i.e., six neighbors), the rewiring frequency f effects the range of intralayer and interlayer synchronization less

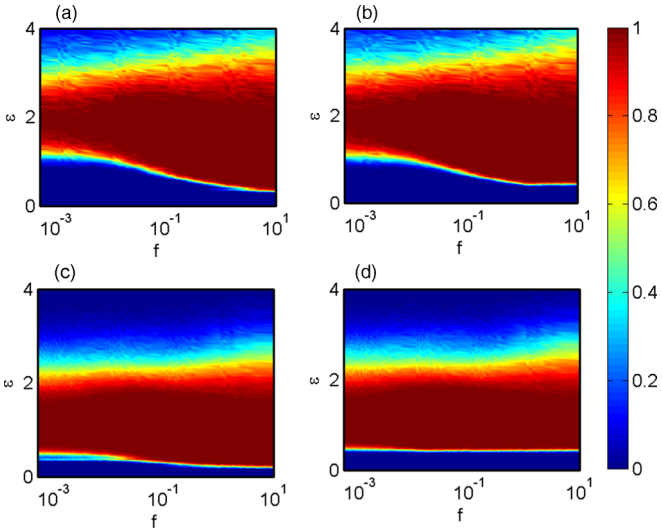

FIG. 5. Basin stability in the f-ϵ plane where $\lambda = \frac{\epsilon}{6}$, for intralayer synchronization where (a) $k = 2$ and (c) $k = 3$; interlayer synchronization where (b) $k = 2$ and (d) $k = 3$.

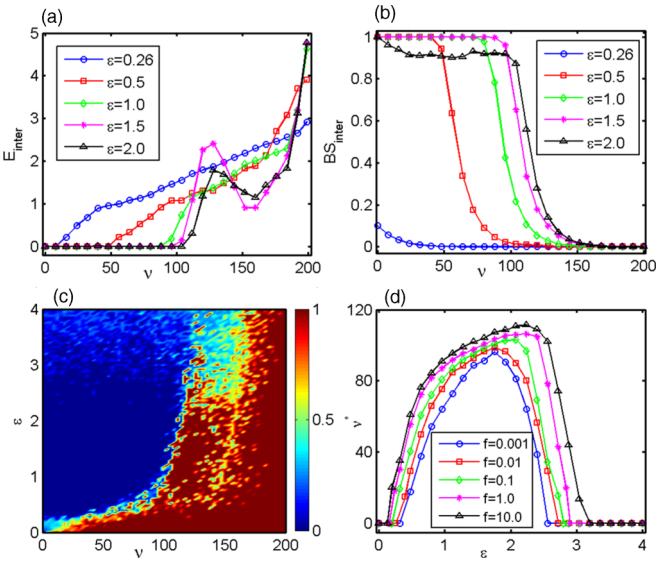

FIG. 6. Variation of (a) interlayer synchronization error and (b) corresponding basin stability with respect to the number of demultiplexed nodes ν for various intralayer coupling strength $\epsilon = 0.26$ (blue circle), 0.5 (red square), 1.0 (green diamond), 1.5 (magenta star), and 2.0 (black triangle). (c) Phase diagram in the ν-ϵ plane for interlayer synchronization for $f = 0.1$ and $\lambda = 0.2$. (d) Maximum number of demultiplexed nodes ν^* preserving interlayer synchrony against increasing ϵ for various rewiring frequencies $f = 0.001$ (blue circle), 0.01 (red square), 0.1 (green diamond), 1.0 (magenta star), and 10 (black triangle). Here $\lambda = 0.2$.

significantly, as is evident from Figs. 5(c) and 5(d). This implies that when the coupling does not extend over a large range, the rewired links can assist the onset of synchronization. The underlying reason for this is that switching links rapidly allows a larger number of sites to be affected by the state of a single site, leading to enhanced information propagation in the system. This naturally helps to synchronize the network. Lastly, we can also observe from Fig. 5 that the lower critical values of ϵ at which intralayer and interlayer synchronizations emerge in the network decrease for a larger number of neighbors k, as is clearly discernible from the figures for $k = 2$ and 3. This is in accordance with the general trend observed in many complex systems that a larger range of coupling interaction aids synchronization, as it entails that information can propagate over a larger neighborhood in less time.

C. Effect of demultiplexing

Lastly, we investigate the robustness of interlayer synchronization against progressive random demultiplexing in the network architecture. So starting from a complete multiplex structure, we sequentially remove the replicas connecting the multiplex nodes until the two layers become completely uncoupled. Figure 6(a) shows the interlayer synchronization error E_{inter} with respect to the number of demultiplexed nodes ν, starting from 0 to the limiting case of $N = 200$, for different values of intralayer coupling strength ϵ and fixed interlayer coupling strength ($\lambda = 0.20$) and rewiring frequency ($f = 0.1$). For $\epsilon = 0.26$, E_{inter} becomes nonzero at a fairly low value of $\nu = 15$. That is, when only 15 interlayer links

connecting the replicas between the layers were removed, the network lost interlayer synchronization. But at a higher value of intralayer coupling strength ϵ, for instance $\epsilon = 0.5$, E_{inter} remains zero even when $\nu = 53$. Also, for high intralayer coupling strengths, interlayer synchronization is preserved even when a large number of interlayer links are disconnected. So for increasing intralayer interaction strengths up to $\epsilon \sim 2.0$, the critical value of ν needed for interlayer desynchronization increases gradually, and *interlayer synchronization persists even when* 50% *of the interlayer links are removed*. Remarkably, the BS measure of global stability indicates that interlayer synchronization persists for a fraction of random initial conditions even when 75% of the interlayer links are demultiplexed, for high intralayer coupling strength ϵ [cf. Fig. 6(b)]. That is, interlayer synchronization still persists for a large set of initial conditions even after a large number of interlayer links have been removed. After a critical ν, however, the interlayer synchronization decreases sharply. So Fig. 6(b) is suggestive of a phase transition from interlayer synchronization to a desynchronized state with respect to an increasing number of removed links.

To illustrate the effect of the intralayer coupling strength ϵ on the interlayer synchrony for continuous demultiplexing of the network, we plot the interlayer synchronization error E_{inter} in the ν-ϵ plane in Fig. 6(c). The figure explicitly demonstrates that the critical value of ν up to which interlayer synchrony is supported improves considerably as ϵ increases. By increasing the intralayer coupling strength, the number of interlayer links that may be removed increases while interlayer synchrony is still preserved. This trend continues up to a certain limit, and increasing ϵ beyond this limit decreases the critical value of ν.

Finally, we show the maximum (or critical) number of demultiplexed links ν^*, which allow interlayer synchronization, as a function of intralayer coupling strength ϵ, for different rewiring frequencies f. Higher ν^* indicates greater robustness of interlayer synchronization with respect to progressive demultiplexing. Notably, here again the rewiring frequency f crucially influences ν^*, whereas there was no effect of rewiring frequencies on interlayer synchronization for the complete multiplex network structure. For small f, with increasing ϵ, ν^* initially grows as well. After a certain value of ϵ, ν^* starts declining and finally becomes zero again. Higher frequencies of rewiring yield larger values of ν^*. This implies that *increasing only the frequency of switching links in the layers, one can make the interlayer synchrony more persistent*, with stable interlayer synchronization persisting even when a large number of replica nodes are disconnected in the network. Further, ν^* again first increases from zero to a limiting large value, and then after a window of coupling strength it decreases to zero again. So the nonmonotonic dependence of ν^* on ϵ holds for all values of f.

IV. CONCLUSIONS

In conclusion, we have studied the stability of intralayer and interlayer synchronization in a multiplex network, where each layer is represented by small-world networks whose links vary over time while the interlayer connections are static. Using linear stability analysis, we derived analytically the necessary condition for intralayer and interlayer synchronization states. To quantify the stability of these two synchronous states in a global sense, we take the basin stability approach. Significantly, the critical value of the intralayer coupling strength for intralayer synchronization is much lower when the links in the layers change more rapidly, while the critical interlayer coupling threshold is almost the same for all rewiring frequencies. We further explored the robustness of the interlayer synchronous state against progressive demultiplexing of the replica nodes. Interestingly, we found that interlayer synchronization persists even when a large number of nodes are demultiplexed if the intralayer connections change rapidly. So increasing only the frequency of switching links in the layers allows the interlayer synchrony to be more persistent, and this may have potential applications in increasing the synchrony of the layers in a multiplex network.

ACKNOWLEDGMENTS

D.G. was supported by SERB-DST (Department of Science and Technology), Government of India (Project No. EMR/2016/001039).

[1] P. Holme and J. Saramäki, Phys. Rep. **519**, 97 (2012).
[2] S. Wasserman and K. Faust, *Social Network Analysis: Methods and Applications* (Cambridge University Press, Cambridge, 1994).
[3] R. Pastor-Satorras and A. Vespignani, *Evolution and Structure of the Internet: A Statistical Physics Approach* (Cambridge University Press, Cambridge, 2004).
[4] I. V. Belykh, V. N. Belykh, and M. Hasler, Physica D **195**, 188 (2004).
[5] V. Kohar, P. Ji, A. Choudhary, S. Sinha, and J. Kurths, Phys. Rev. E **90**, 022812 (2014).
[6] A. Mondal, S. Sinha, and J. Kurths, Phys. Rev. E **78**, 066209 (2008).
[7] J. Lü and G. Chen, IEEE Trans. Autom. Control **50**, 841 (2005).
[8] M. Frasca, A. Buscarino, A. Rizzo, L. Fortuna, and S. Boccaletti, Phys. Rev. Lett. **100**, 044102 (2008); L. Prignano, O. Sagarra, and A. Díaz-Guilera, *ibid.* **110**, 114101 (2013).
[9] S. Majhi and D. Ghosh, Chaos **27**, 053115 (2017).
[10] D. Levis, I. Pagonabarraga, and A. Díaz-Guilera, Phys. Rev. X **7**, 011028 (2017).
[11] R. Olfati-Saber, J. A. Fax, and R. M. Murray, Proc. IEEE **95**, 215 (2007).
[12] V. Kohar, and S. Sinha, Chaos Solitons Fractals **54**, 127 (2013).
[13] M. L. Sachtjen, B. A. Carreras, and V. E. Lynch, Phys. Rev. E **61**, 4877 (2000).
[14] M. Valencia, J. Martinerie, S. Dupont, and M. Chavez, Phys. Rev. E **77**, 050905(R) (2008).
[15] J. P. Onnela, J. Saramaki, J. Hyvonen, G. Szabo, D. Lazer, K. Kaski, J. Kertesz, and A. L. Barabasi, Proc. Natl. Acad. Sci. (U.S.A.) **104**, 7332 (2007); Y. Wu, C. Zhou, J. Xiao, J. Kurths, and H. J. Schellnhuber, *ibid.* **107**, 18803 (2010); J. L. Iribarren, and E. Moro, Phys. Rev. Lett. **103**, 038702 (2009).
[16] D. Tanaka, Phys. Rev. Lett. **99**, 134103 (2007).
[17] F. Sivrikaya and B. Yener, IEEE Network **18**, 45 (2004).

[18] S. Boccaletti, G. Bianconi, R. Criado, C. I. del Genio, J. Gómez-Gardeñes, M. Romance, I. Sendiña-Nadal, Z. Wang, and M. Zanin, Phys. Rep. **544**, 1 (2014).
[19] M. Kivelä, A. Arenas, M. Barthelemy, J. P. Gleeson, Y. Moreno, and M. A. Porter, J. Complex Netw. **2**, 203 (2014).
[20] M. Szell, R. Lambiotte, and S. Thurner, Proc. Natl. Acad. Sci. (U.S.A.) **107**, 13636 (2010).
[21] A. Cardillo, J. Gómez-Gardeñes, M. Zanin, M. Romance, D. Papo, F. del Pozo, and S. Boccaletti, Sci. Rep. **3**, 1344 (2013); A. Halu, S. Mukherjee, and G. Bianconi, Phys. Rev. E **89**, 012806 (2014).
[22] A. Cardillo, M. Zanin, J. Gómez-Gardeñes, M. Romance, A. García del Amo, and S. Boccaletti, Eur. Phys. J. Spec. Top. **215**, 23 (2013).
[23] R. Criado, M. Romance, and M. Vela-Pérez, Int. J. Bifurcation Chaos **20**, 877 (2010); R. Criado, B. Hernández-Bermejo, and M. Romance, *ibid.* **17**, 2289 (2007).
[24] B. M. Adhikari, A. Prasad, and M. Dhamala, Chaos **21**, 023116 (2011).
[25] F. Radicchi and A. Arenas, Nat. Phys. **9**, 717 (2013).
[26] J. Gómez-Gardeñes, M. De Domenico, G. Gutiérrez, A. Arenas, and S. Gómez, Philos. Trans. A Math. Phys. Eng. Sci. **373**, 20150117 (2015).
[27] A. Saumell-Mendiola, M. Á. Serrano, and M. Boguna, Phys. Rev. E **86**, 026106 (2012).
[28] C. Granell, S. Gómez, and A. Arenas, Phys. Rev. Lett. **111**, 128701 (2013).
[29] C. Buono, L. G. Alvarez-Zuzek, P. A. Macri, and L. A. Braunstein, PLoS One **9**, e92200 (2014).
[30] J. Sanz, C.-Y. Xia, S. Meloni, and Y. Moreno, Phys. Rev. X **4**, 041005 (2014).
[31] S. Gómez, A. Díaz-Guilera, J. Gómez-Gardeñes, C. J. Pérez-Vicente, Y. Moreno, and A. Arenas, Phys. Rev. Lett. **110**, 028701 (2013).
[32] G. Menichetti, L. DallAsta, and G. Bianconi, Sci. Rep. **6**, 20706 (2016).
[33] S. V. Buldyrev, R. Parshani, G. Paul, H. E. Stanley, and S. Havlin, Nature (London) **464**, 1025 (2010); J. Gao, S. V. Buldyrev, H. E. Stanley, and S. Havlin, Nat. Phys. **8**, 40 (2012).
[34] G. Bianconi and S. N. Dorogovtsev, Phys. Rev. E **89**, 062814 (2014).
[35] Z. Wang, A. Szolnoki, and M. Perc, J. Theor. Biol. **349**, 50 (2014).
[36] R. G. Morris and M. Barthelemy, Phys. Rev. Lett. **109**, 128703 (2012).
[37] X. Zhang, S. Boccaletti, S. Guan, and Z. Liu, Phys. Rev. Lett. **114**, 038701 (2015).
[38] L. V. Gambuzza, M. Frasca, and J. Gómez-Gardeñes, Europhys. Lett. **110**, 20010 (2015).
[39] R. Sevilla-Escoboza, I. Sendiña-Nadal, I. Leyva, R. Gutiérrez, J. M. Buldú, and S. Boccaletti, Chaos **26**, 065304 (2016).
[40] I. Leyva, R. Sevilla-Escoboza, I. Sendiña-Nadal, R. Gutiérrez, J. M. Buldú, and S. Boccaletti, Sci. Rep. **7**, 45475 (2017).
[41] S. Jalan and A. Singh, Europhys. Lett. **113**, 30002 (2016).
[42] V. A. Maksimenko, V. V. Makarov, B. K. Bera, D. Ghosh, S. K. Dana, M. V. Goremyko, N. S. Frolov, A. A. Koronovskii, and A. E. Hramov, Phys. Rev. E **94**, 052205 (2016).
[43] S. Majhi, M. Perc, and D. Ghosh, Sci. Rep. **6**, 39033 (2016).
[44] S. Majhi, M. Perc, and D. Ghosh, Chaos **27**, 073109 (2017).
[45] V. H. P. Louzada, N. Araújo, J. S. Andrade, and H. J. Herrmann, Sci. Rep. **3**, 3289 (2013).
[46] R. Sevilla-Escoboza, R. Gutiérrez, G. Huerta-Cuellar, S. Boccaletti, J. Gómez-Gardeñes, A. Arenas, and J. M. Buldú, Phys. Rev. E **92**, 032804 (2015).
[47] R. Gutiérrez, I. Sendiña-Nadal, M. Zanin, D. Papo, and S. Boccaletti, Sci. Rep. **2**, 396 (2012).
[48] A. Bogojeska, S. Filiposka, I. Mishkovski, and L. Kocarev, Telecommun. Forum (TELFOR), **2013** 21st, 172 (2013).
[49] J. Aguirre, R. Sevilla-Escoboza, R. Gutiérrez, D. Papo, and J. M. Buldú, Phys. Rev. Lett. **112**, 248701 (2014).
[50] E. Ubaldi, A. Vezzani, M. Karsai, N. Perra, and R. Burioni, Sci. Rep. **7**, 46225 (2017).
[51] M. Starnini, A. Machens, C. Cattuto, A. Barrat, and R. Pastor-Satorras, J. Theor. Bio. **337**, 89 (2013).
[52] P. J. Menck, J. Heitzig, N. Marwan, and J. Kurths, Nat. Phys. **9**, 89 (2013).
[53] S. Leng, W. Lin, and J. Kurths, Sci. Rep. **6**, 21449 (2016).
[54] S. Rakshit, B. K. Bera, S. Majhi, C. Hens, and D. Ghosh, Sci. Rep. **7**, 45909 (2017).
[55] S. Rakshit, B. K. Bera, M. Perc, and D. Ghosh, Sci. Rep. **7**, 2412 (2017).
[56] D. J. Watts and S. H. Strogatz, Nature (London) **393**, 440 (1998).
[57] J. F. Heagy, L. M. Pecora, and T. L. Carroll, Phys. Rev. Lett. **74**, 4185 (1995).